AGU PUBLICATIONS

Geophysical Research Letters

RESEARCH LETTER
10.1002/2016GL068784

Key Points:
- How does the ocean control the melting of Greenland glaciers?
- Glaciers dominated by calving processes are less sensitive to ice-ocean interactions
- The study provided a basis for quantifying ice-ocean interaction elsewhere around Greenland

Supporting Information:
- Supporting Information S1

Correspondence to:
E. Rignot,
erignot@uci.edu

Citation:
Rignot, E., et al. (2016), Modeling of ocean-induced ice melt rates of five west Greenland glaciers over the past two decades, *Geophys. Res. Lett.*, *43*, 6374–6382, doi:10.1002/2016GL068784.

Received 25 MAR 2016
Accepted 25 MAY 2016
Accepted article online 30 MAY 2016
Published online 24 JUN 2016

Modeling of ocean-induced ice melt rates of five west Greenland glaciers over the past two decades

E. Rignot[1,2], Y. Xu[1], D. Menemenlis[2], J. Mouginot[1], B. Scheuchl[1], X. Li[1], M. Morlighem[1], H. Seroussi[1], M. van den Broeke[3], I. Fenty[2], C. Cai[1], L. An[1], and B. de Fleurian[1]

[1]Department of Earth System Science, University of California, Irvine, California, USA, [2]Jet Propulsion Laboratory, California Institute of Technology, Pasadena, California, USA, [3]Institute for Marine and Atmospheric Research, Utrecht University, Utrecht, Netherlands

Abstract High-resolution, three-dimensional simulations from the Massachusetts Institute of Technology general circulation model ocean model are used to calculate the subaqueous melt rate of the calving faces of Umiamako, Rinks, Kangerdlugssup, Store, and Kangilerngata glaciers, west Greenland, from 1992 to 2015. Model forcing is from monthly reconstructions of ocean state and ice sheet runoff. Results are analyzed in combination with observations of bathymetry, bed elevation, ice front retreat, and glacier speed. We calculate that subaqueous melt rates are 2–3 times larger in summer compared to winter and doubled in magnitude since the 1990s due to enhanced subglacial runoff and 1.6 ± 0.3°C warmer ocean temperature. Umiamako and Kangilerngata retreated rapidly in the 2000s when subaqueous melt rates exceeded the calving rates and ice front retreated to deeper bed elevation. In contrast, Store, Kangerdlugssup, and Rinks have remained stable because their subaqueous melt rates are 3–4 times lower than their calving rates, i.e., the glaciers are dominated by calving processes.

1. Introduction

The Greenland Ice Sheet has been experiencing an accelerating rate of mass loss over the past few decades from a combination of enhanced surface melt and increased glacier ice discharge [e.g., *Rignot and Kanagaratnam*, 2006; *van den Broeke et al.*, 2009; *Enderlin et al.*, 2014]. Widespread acceleration of its marine-terminating glaciers and fluctuations in the position of their calving margins has been attributed to the enhanced advection of warm subsurface ocean waters of subtropical origin at the ice-ocean boundary [e.g., *Holland et al.*, 2008; *Rignot et al.*, 2010; *Straneo et al.*, 2010; *Rignot et al.*, 2012; *Bevan et al.*, 2012; *Christoffersen et al.*, 2011]. Yet there has been no quantitative demonstration of the role of subaqueous melt in driving tidewater glaciers into a retreat, in part due to our poor knowledge of the magnitude of the subaqueous melt rates, their spatial pattern, horizontally and vertically, and their seasonal to interannual variability. One hypothesis is that subaqueous melting at the ice front has increased sufficiently in magnitude to counteract the advection of ice from upstream and force the glacier front to retreat. As the glacier retreats, the removal of grounded ice at the ice front will reduce basal resistance, which will enable glacier ice from upstream to speedup. Speedup will cause ice to thin from longitudinal stretching, which will be conducive to further retreat. The retreat rate will depend on the glacier geometry, especially the bed elevation below sea level and whether the bed elevation increases or decreases farther inland [e.g., *Post et al.*, 2011]. When examining the details of the glacier response to ocean thermal forcing, large variations have been reported from one glacier to the next or within the same fjord system [e.g., *Box and Decker*, 2011; *Moon et al.*, 2012], which suggests a complex interplay between subaqueous melting, iceberg calving, glacier geometry, and other factors [*Benn et al.*, 2007].

Here we consider the recent history of five glaciers in central west Greenland for which we have quality data to reconstruct ocean-induced melt rates. We review their time evolution and response to atmospheric and oceanic forcings. We use three-dimensional, high-resolution simulations of ice melt into the ocean to model their horizontal, vertical, seasonal, and interannual variability. Model forcing is constrained using in situ oceanographic data, reconstructions of ice sheet runoff, novel bed topography, and bathymetry data. We compare changes in subaqueous melt rate through time with ice velocity at the ice front. We conclude on the impact of ice-ocean interaction on the glacier dynamics and in turn on glacier stability.

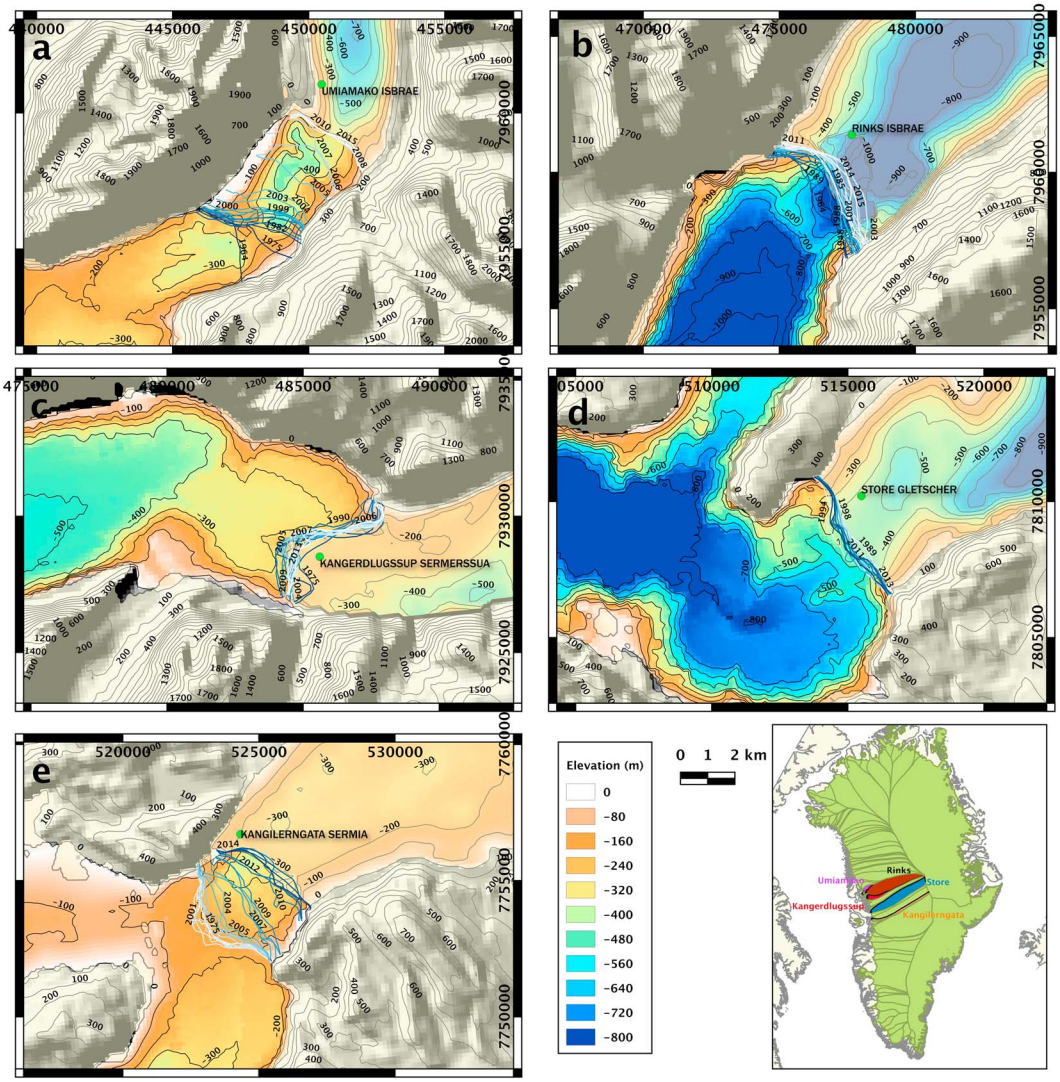

Figure 1. Bed elevation of five Greenland glaciers and bathymetry in the glacial fjords of (a) Umiamako Isbrae, (b) Rinks Isbrae, (c) Kangerdlugssup Sermerssuam, (d) Store Gletscher, and (e) Kangilerngata Sermia. Inset shows the location of the glacier basins in Greenland color coded purple, brown, red, blue, and orange from north to south. Bed elevation and bathymetry contours are every 100 m. Bed elevation on grounded ice is shaded with 52% transparency. Ice front positions from 1964 to 2015 are color coded from blue to white, with black labels.

2. Data and Methods

2.1. Remote Sensing Data

Store Gletscher, Kangerdlugssup Sermerssua, Rinks Isbrae, and Umiamako Isbrae are four tidewater glaciers from the Uummanaak region, in west Greenland (Figure 1a); Kangilerngata Sermia drains into Ata Sund fjord, 50 km to the south (Figure 1). The drainage basin, ice flux, and annual speed of the glaciers are listed in Table 1. Store and Rinks are among the fastest glaciers in Greenland, with large drainage basins; the other two glaciers flow 2–3 times slower, with smaller drainage basins [*Rignot and Mouginot*, 2012].

To conduct our analysis of the glacier evolution, we employ data on ice front position, bed elevation, bathymetry, ice velocity, ocean temperature, and subglacial freshwater discharge from the glaciers. We digitize the ice front positions using airborne imagery from 1964 [*Carbonnell and Bauer*, 1968] and satellite imagery from Landsat-MSS (1976), Landsat-TM (1975–1978), Landsat-5 (1985–1998), Landsat-7 (1999–2012), and Landsat-8 (2013–2015) (Figure 1). The data are from midsummer when the ice fronts are easy to identify but not necessarily at their most retreated position [*Howat et al.*, 2010]. Yearly ice front positions are mapped within 30¨m. Short-term variations average about 100¨m. We calculate an annual retreat rate, q_r, in meter per

Table 1. Characteristics of Five Greenland Tidewater Glaciers[a]

		Q_f	A_f		Q_{sg}			q_m		q_f	q_r
	DB	Gt/yr	km^2		m^3/s			m/d		m/d	m/d
Glacier	km^2	Yr	Yr	W	Yr	Peak	W	S	Peak	Yr	Yr
Umiamako Isbrae	2,304	2.6	0.9	1	16	198	0.6	1.0	2.0	1.3 ± 0.4	0.5 ± 0.8
Rinks Isbrae	33,171	12.7	2.7	13	38	405	1.1	1.6	3.4	8.3 ± 0.5	0.05 ± 0.5
Kangerdlugssup S.	5,000	3.0	1.4	3	39	473	0.6	1.0	2.0	4.5 ± 0.5	0.03 ± 0.3
Store Gletscher	30,507	11.5	1.8	13	99	890	0.8	1.5	3.0	5.2 ± 0.4	-0.02 ± 0.2
Kangilerngata S.	8,004	1.2	0.9	3	57	438	0.4	0.8	1.9	2.0 ± 0.9	0.4 ± 0.8

[a]DB is the drainage basin in square km; Q_f the ice front flux in 2007 in gigatons (10^{12}kg) per year; A_f the mean submerged area in square kilometer; Q_{sg} the mean subglacial water flux in cubic meter per second in winter (W), annual (Yr), and summer peak (peak); and q_m the mean subaqueous melt rate in meter per day in winter (W), summer (S), and summer peak value (peak). q_f and q_r are, respectively, the mean annual speed and annual retreat rate ($\pm 1\sigma$) for the time period 1992 to 2015.

day, by dividing the area of retreat by the glacier width over the 1 year period separating the images. Data separated by a few months or less yield noisy time series of q_r because iceberg calving is not a continuous process like ice motion or ice melt by the ocean.

Glacier bed elevation is from *Morlighem et al.* [2014] combining NASA Operation IceBridge (OIB) thickness data and ice motion vectors from *Rignot and Mouginot* [2012] using a mass conservation (MC) approach that minimizes a cost function that measures the disparity between observed and calculated ice thickness. Bed elevation and ice thickness have a horizontal resolution of 350 m, a vertical precision of 50 m, and a posting of 150 m. The MC bed elevation output products are constrained to match the bathymetry data at the ice-ocean margin by including an additional term in the cost function that minimizes the difference between observed bathymetry at the ice front and calculated bed depth at the ice front. Bathymetry was collected using a Reson 8160 multibeam echo sounder operating at 50 kHz in August 2012 and 2013 (Figure 1), with a 1 m vertical precision, at a 25 m posting [*Rignot et al.*, 2016]. For Umiamako, we extended the MC results using a bed solution for year 1996 when the glacier was at a more advanced position. Combined together, these data help constrain water depth, h.

We use ice velocity data for years 2000 to 2011 from *Joughin et al.* [2010], complemented with ice velocity for year 1989–2015 from Landsat data (*Howat* [2016] and this study), year 1996 from ERS-1 interferometry, and winter 2014 from RADARSAT-2. We calculate a width-averaged ice speed for the glacier fronts, q_f, in meter per day. The precision of q_f is 1 m/yr for 2000–2015, 2–3 m/yr for 1996, and 15 m/yr for Landsat data prior to 2013. We generate annual averages in ice velocity to minimize data noise.

2.2. ECCO Ocean Thermal Forcing

The amount of ocean heat delivered to the glacier to melt ice is proportional to the difference in temperature between the potential temperature of seawater and the pressure-dependent freezing point of seawater or ocean thermal forcing, *TF*. We calculate a vertically averaged TF between 200 m depth and the depth of the seafloor in front of the glacier. Ocean model simulations show that it is approximately over that depth range ($\pm$50 m) than ice melts and melt water mixes with ocean waters [*Xu et al.*, 2013]. Ocean temperature is from an ocean simulation carried out by the Estimating the Circulation and Climate of the Ocean, Phase II (ECCO2) project at 4 km horizontal spacing [*Nguyen et al.*, 2012] based on the optimized coarser-resolution configuration of *Losch et al.* [2010] and *Nguyen et al.* [2011]. Due to the coarse resolution of the ECCO2 simulation and the uncertainty of the bathymetry data used by ECCO2, we extract a mean ocean temperature profile for the entire Uummannaq fjord. A comparison of ECCO2 model results with long-term temperature data from the Labrador and Irminger Seas was reported in *Rignot et al.* [2012] and showed a +0.4°C bias. Here we use conductivity-temperature-depth (CTD) data collected in years 2007 [*Weinrebe et al.*, 2009], 2008, 2009–2010 [*Chauche et al.*, 2014], 2011, 2012, 2013, and 2014 to compare ECCO2 temperature and observations (Figure 2). We adjust the ECCO2 model results using the CTD data from year 2013 only. The adjustment is 0.1°C for Umiamako, Rink, and Kangerdlugssup; 0.2°C for Store; and 0.7°C for Kangilernata. We calculate a mean difference in TF between ECCO2 and all CTD data of 0.2°C. If we vary the minimum depth of TF by $\pm$50 m, we find

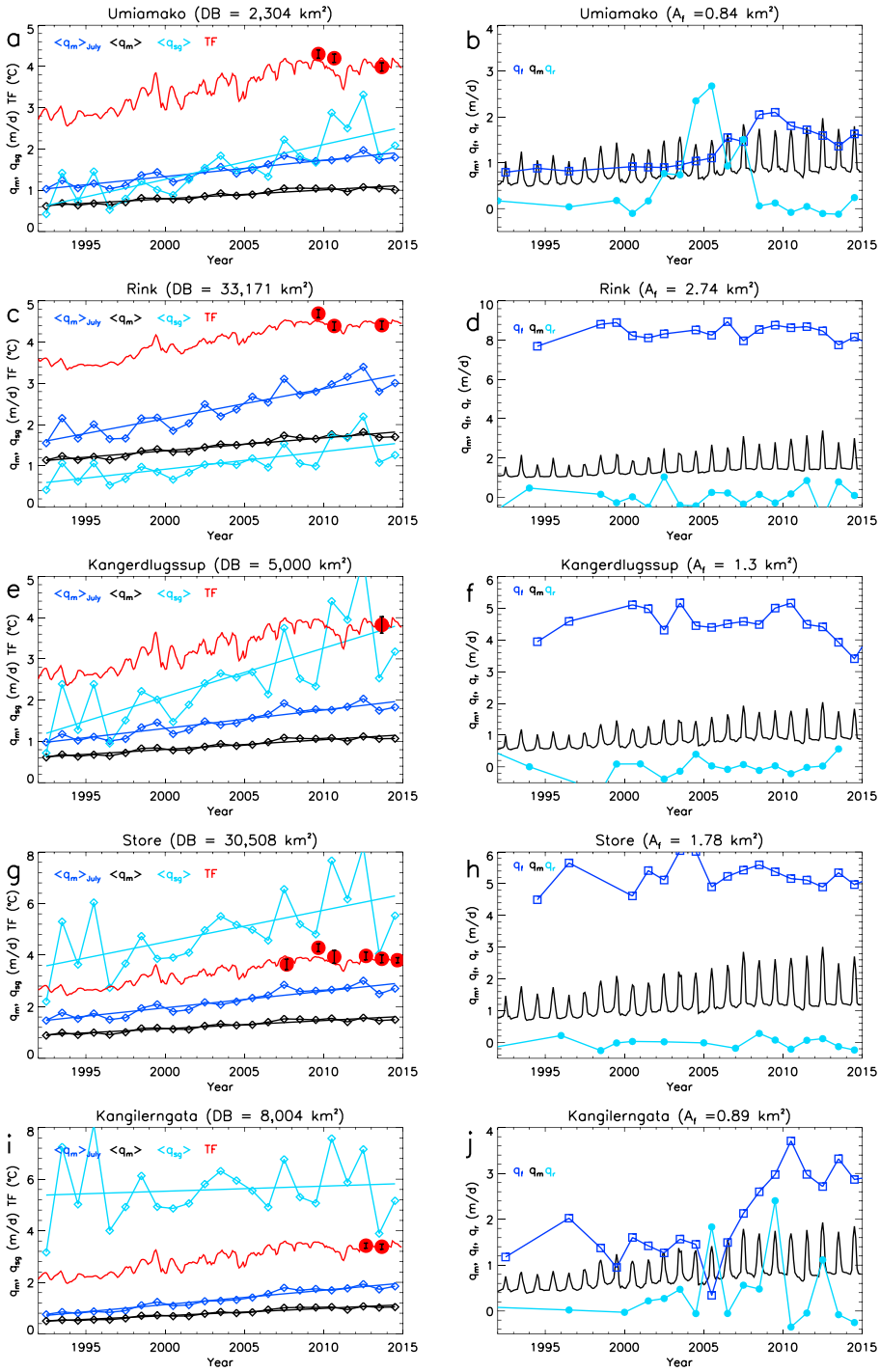

Figure 2. Evolution of the subaqueous melt rate q_m of five Greenland glaciers: (a, b) Umiamako Isbrae, (c, d) Rinks Isbrae, (e, f) Kangerdlugssup Sermerssuam, (g, h) Store Gletscher, and (i, j) Kangilerngata Sermia. Figures 2a, 2c, 2e, and 2g show the annual effective subglacial water discharge (light blue diamond), $< q_{sg} >$, the summer (July) subaqueous melt rate (dark blue diamond), $< q_m >_{July}$, the annual subaqueous melt rate (black diamond), $< q_m >$, and their corresponding linear fit from 1992 to 2015, in meter per day. Ocean thermal forcing, TF, in degree Celsius is red. Solid red circles denote CTD temperature data from year 2007 to 2014. DB is the drainage basin area in square kilometers. Figures 2b, 2d, 2f, and 2h show the monthly ice speeds (dark blue square with thin line in between measurements), q_f, the monthly subaqueous melt rate (black curve), q_m, and the yearly glacier retreat rate (light blue circle with thin line in between measurements), q_r, from 1992 to 2015, in meter per day. A_f is the ice front submerged area in square kilometers.

an uncertainty of 0.1°C in the CTD values for Umiamako, Rink, and Kangilernata and 0.2°C for Kangerdlugssup and Store. In total, we estimate a mean uncertainty in TF of 0.3°C.

The thermohaline circulation that takes place in front of the marine-terminating glaciers depends on the subglacial freshwater flux, Q_{sg}, delivered at the glacier base. Q_{sg} includes (1) ice sheet surface runoff and (2) subglacial melt from geothermal heat and basal friction. Ice sheet runoff is from the Regional Atmospheric Climate Model (RACMO2), with a precision of 20% [*Ettema et al.*, 2009; *van Angelen et al.*, 2012]. In summer, this is the dominant source of subglacial water. In winter, melting of grounded ice dominates. We calculate it using a numerical model of the thermal state of the Greenland Ice Sheet that employs the enthalpy method [*Aschwanden et al.*, 2012]. The model setup is identical to that in *Seroussi et al.* [2013], updated after evaluating the enthalpy framework following *Kleiner et al.* [2015]. The ice sheet runoff and grounded ice basal melt water production are integrated over the glacier surface drainage, i.e., assuming that the subglacial water drainage coincides with the surface drainage, to obtain basin-wide estimates of Q_{sg} in cubic meter per second. We deduce an effective subglacial freshwater velocity, q_{sg}, in meter per day, by dividing Q_{sg} by the submerged area of the ice front, derived from the bathymetry mapping, hence is time dependent, and updated annually (Table 1). q_{sg} is expressed in the same unit as q_f and q_m and differs from the unknown speed of subglacial flow within the channelized system at the ice front.

2.3. Ocean Model

We model subaqueous melting of a 150 m wide, vertical, ice face standing in ocean water with subglacial freshwater discharge using the Massachusetts Institute of Technology general circulation model (MITgcm), with a free surface, nonhydrostatic conditions, in three dimensions and at a 1 m spatial resolution sufficient to generate plume turbulence [*Xu et al.*, 2013]. The fjord is rectangular in shape and extends 500 m from the ice front (supporting information). The subglacial discharge is injected at the glacier base via a fixed-size cavity and imposed as a net influx of cold, fresh water mass. Simulations indicate that the exact shape and distribution of subglacial cavities only modulate the area-average melt rate by ±15% keeping the subglacial water flux constant [*Xu et al.*, 2013]. *Slater et al.* [2015] report a larger variability in melt rates for the more extreme cases of fully channelized and fully distributed systems. Most subglacial water is, however, discharged from 1–2 main channels and a series of smaller channels [*Rignot et al.*, 2015; *Fried et al.*, 2015], which is a configuration similar to *Xu et al.* [2013]. Here we assume an uncertainty of 15% but recognize that the uncertainty could be larger.

From the MITgcm simulations, we calculate the effective ocean-induced melt speed, q_m, in meter per day, as the horizontally averaged, maximum rate of ice melt. q_m is not the area-averaged ice melt rate as in *Xu et al.* [2013] because the melt rate is not uniform with depth. The melt rate reaches a maximum value in the lower part of the ice face, hence creating conditions for ice front undercutting [*Rignot et al.*, 2015; *Luckman et al.*, 2015; *O'Leary and Christoffersen*, 2013]. It is the rate of deep undercutting caused by the ocean waters that controls the migration back and forth of the ice front, not the area-average melt rate or melt rate near the surface. Undercutting has been observed using multibeam echo soundings of calving faces [*Rignot et al.*, 2015; *Fried et al.*, 2015] and confirmed to be a significant driver of iceberg calving for tidewater glaciers [*Luckman et al.*, 2015]. Ice below the region of undercutting will exert negligible basal friction because it is too thin (10–100 m). We calculate q_m for various values of TF, q_{sg}, and water depth, h, and use a simple model fit to match the results (Table S1 in the supporting information). We then find a formulation that unifies all the simulations together using a generalization of the model fit used by *Xu et al.* [2013] as

$$q_m = (A \;\; h \;\; q_{sg}^{\alpha} + B) \;\; \mathrm{TF}^{\beta} \tag{1}$$

with $A = 3 \times 10^{-4}$ units, h is water depth in meter, q_{sg} the subglacial water flux in m/d, $\alpha = 0.39$, $B = 0.15$ units, TF is the thermal forcing, and $\beta = 1.18$ (Figure S1). B expresses that q_m is nonzero in the absence of subglacial water flux. TF depends on water depth via the pressure-dependent freezing point of seawater. We find that the model fit agrees with the simulations within 0.2 m/d or 7% (Figure S2).

The uncertainty in q_m includes a 20% uncertainty in q_{sg} (scaled by α in equation (1)) and a 0.3°C uncertainty in TF or 5% (scaled by β), which amounts to a 14% uncertainty from equation (1). We combine this error quadratically with a 15% error due to the unknown shape and spatial distribution of subglacial channels [*Xu et al.*, 2013], a 5% error in submerged cross-section submerged ice front area, and a 7% uncertainty due to the model fit (Figure S2). We estimate the total uncertainty in q_m to be 26%.

Given q_{sg}, TF, and h, we calculate monthly values of q_m using equation (1) taking into account changes in position of the ice front and water depth. We then compare the effective melt speed, q_m, with the average glacier ice front speed, q_f, and the annual rate of ice front retreat, q_r, which balance the calving speed, q_c, as

$$q_r = q_f - q_c - q_m \tag{2}$$

The calving speed, q_c, here represents the dry rate of iceberg calving that would take place in the absence of ocean melt. Calving by undercutting is included in q_m since it is the maximum melt rate at depth. If calving and ocean-induced melt balance q_f exactly, then the glacier front position is steady, i.e., $q_r = 0$. If q_m increases, for instance, with warmer ocean waters or higher subglacial runoff, the glacier front will retreat ($q_r < 0$) unless q_f increases.

3. Results

We describe the glacier geometry, retreat rate, and subglacial runoff; calculated ocean-induced melt rate; and compare the results of the glacier speed. Umiamako Isbrae flows down a 4 km wide valley with a 200 m deep sill at the mouth of the fjord where the glacier front was anchored as far back as the 1850s [*Weidick*, 1968] (Figure 1a). The fjord is up to 300 m deep at the 1964 ice front and up to 350 m deep at the 2012 ice front. Another 5 km upstream, the bed drops to 680 m below sea level. The ice front that retreated 1.5 km from 1964 to 1985 along its southern flank was stable until 2002, retreated by 3.7 km from 2002 to 2008, and has remained stable since.

Rinks Isbrae flows down a 6 km wide valley with steep walls (Figure 1b). The fjord is more than 1000 m deep, with a 650 m deep sill near the ice front. The central part of the glacier is near floatation but is treated here as a near-vertical calving face equivalent. The ice front migrated back and forth with large calving events but remains within 1 km of the 1964 position. Kangerdlugssup is 5 km wide and terminates in waters 350 m deep (Figure 1c). About 6 km inland of the ice front, bed elevation drops by 250 m. The glacier front did not migrate at a significant level between 1964 and 2015. Store is grounded on a 500 m deep sill, several kilometers in length by 5 km in width (Figure 1d). The glacier front has been stable since 1964 and even 1850 [*Weidick*, 1968].

Kangilerngata Sermia is grounded 350 m below sea level in a 3.5 km wide valley (Figure 1e). We detect a sill at 150 m depth about 3 km from the current ice front, where the glacier was grounded from 1964 to 2004 and even in 1920 [*Weidick*, 1968]. The glacier front retreated by 3 km in 2005–2010 and has stabilized since. The bed elevation remains 200–450 m below sea level for 30 km inland of the current ice front position.

Subglacial runoff has increased on all glaciers during the observation period, almost linearly, with large interannual variations (Figure 2). Runoff flux peaked in 2012 but returned to normal in 2013–2014. Winter (no runoff) subglacial flux Q_{sg} is 1, 13, 3, 13, and 3 m^3/s for, respectively, Umiamako, Rinks, Kangerdlugssup, Store, and Kangilerngata (Table 1). Summer (month of July) Q_{sg} is 1–2 orders of magnitude larger. At Umiamako, Q_{sg} peaks at 198 m^3/s in summer and averages 16 m^3/s for the year. The yearly and peak values for Rinks are 38 and 405 m^3/s, 39 and 473 m^3/s for Kangerdlugssup, 99 and 890 m^3/s for Store, and 57 and 438 m^3/s for Kangilerngata. Subglacial water flux varies from year to year but increased by 0.7 $m^3/s/yr$ for Umiamako or 96%, 1.4 $m^3/s/yr$ for Rinks or 81%, 1.7 $m^3/s/yr$ for Kangerdlugssup or 96%, 2.6 $m^3/s/yr$ for Store or 58%, and 1.3 $m^3/s/yr$ for Kangilerngata or 50% in 22 years. During the same period, ocean thermal forcing deduced from ECCO2 increased by 1.5°C from 2.6 to 4.1°C at Store, 1.6°C from 2.1 to 3.7°C at Kangilerngata, 2.7 to 4.3°C at Umiamako, 2.5 to 4.1°C at Kangerdlugssup, and 1.3°C from 3.4 to 4.7°C at Rinks (Figure 2).

As a result of the increase in q_{sg} and TF, we find that q_m increased significantly during the 1992–2014 time period (Figure 2). The melt rate increased from 0.6 to 1.0 m/d in winter due to the increase in TF for Umiamako. The summer melt rate increased from 0.9 to 2.0 m/d. For Rinks, the rate increased from 1.0 to 1.5 m/d in winter and 1.4 to 3.3 m/d in summer. For Kangerdlugssup, the rate increased from 0.6 to 0.9 m/d in winter and 1.0 to 1.9 m/d in summer. For Store, the winter rate increased from 0.8 to 1.2 m/d and the summer rate from 1.5 to 2.8 m/d. For Kangilerngata, the rate increased from 0.4 to 0.9 m/d in winter and 0.7 to 1.9 m/d in summer. The annual melt rate doubled for Kangilerngata from 0.5 to 1 m/d as the glacier retreated into deeper waters and doubled for the other glaciers: 0.6 to 1.1 m/d for Umiamako, 1.1 to 1.8 m/d for Rinks, 0.7 to 1.1 m/d for Kangerdlugssup, and 0.9 to 1.6 m/d for Store.

At Kangilerngata, the ice front speed, q_f, which averaged 2.0 ± 0.8 m/d in 1992–2014, doubled from 1.5 m/d in the 1990s to 2.6 m/d in the last 5 years. At Rinks, Kangerdlugssup, and Store, q_f remained at, respectively,

8.3 ± 0.5, 4.5 ± 0.5, and 5.2 ± 0.3 m/d, with no temporal trend. At Umiamako, q_f averaged 1.1 ± 0.4 m/d in 1992–2014 but increased from 0.8 m/d in the 1990s to 1.8 m/d in 2009 before dropping back to 1.1 m/d in 2013–2014.

Comparing q_m and q_f, we find that q_f for Rinks is 5 times larger than the summer rate q_m. The increase in q_m brought it to within 40% of q_f, but q_m never exceeded q_f. For Store and Kangerdlugssup, q_f is 3 times larger than the summer q_m. For these three glaciers, the changes in frontal ablation are clearly dominated by calving processes, not by ocean-induced ice melt. In contrast, the summer q_m for Kangilerngata exceed q_f around 2002 until 2010. For Umiamako, q_m was comparable to q_f for several years starting in the early 2000s. For these glaciers, changes in frontal ablation are dominated by submarine melting.

The ice fronts of Rinks, Kangerdlugssup, and Store did not migrate more than ±230 m since 1992, q_f did not change, and the increase in q_m had no impact on the glacier stability. In contrast, Umiamako and Kangilerngata retreated by 4.2 and 3.3 km, respectively, in 1992–2015. Most of the retreat of Umiamako took place between 2002 and 2008, when the glacier retreated into a bed about 50 m deeper below sea level. Kangilerngata retreated 2.3 km between 2005 and 2010, from a bed 150 m below sea level to a bed 350 m below sea level.

4. Discussion

The model simulations suggest significant fluctuations in melt rate between summer and winter. This is due to the net decrease in subglacial water flux in winter, which reduces the strength of the thermohaline circulation along the ice face. Winter melt rates are 2 times lower than the summer melt rates. Ice front retreat is therefore more likely to occur in the summer months when the melt rates are the highest, especially since ice front speeds only increase by 8–10% in summer compared to winter [*Rignot and Kanagaratnam*, 2006]. This implies that subglacial runoff, and therefore higher air temperature, exerts an indirect important control on the rate of subaqueous melt. On the other hand, the relatively high values modeled in winter indicate that ice melt by the ocean is a year-round phenomena, i.e., winter rates should not be neglected.

Few observations of ice melt rate have been obtained in Greenland [*Rignot et al.*, 2010; *Motyka et al.*, 2011; *Sutherland and Straneo*, 2012; *Xu et al.*, 2013; *Enderlin and Howat*, 2013; *Fried et al.*, 2015]. Our calculated values are within the range of those obtained in the field in Greenland over a period of a few days, i.e., 0.5 m/d to 4 m/d. *Fried et al.* [2015] quote an average melt rate of 1.6 m/d in July 2013 for Kangerdlugssup versus 1.8 ± 0.5 m/d in our model. For Store, our summer results of 3.0±0.8 m/d for July 2012 are consistent with the hydrographic estimate of 3.0 ± 1 m/d by *Xu et al.* [2013]. For Rinks, *Enderlin and Howat* [2013] estimate summer melt rates of 2.1 to 2.5 m/d in 2000–2008 from remote sensing versus 3.4 ± 0.8 m/d for July and 1.8 m/d for June–September in our simulation. For Kangilerngata, *Rignot et al.* [2010] estimated 2.6 ± 0.5 m/d in July and August 2008 versus 1.9 ± 0.4 m/d herein.

The model simulations indicate that q_m has increased significantly over the past decades as a result of an increase in q_{sg}, TF, and water depth, h. The change in submerged area had only a small contribution to the change in q_m. The change in water depth enhanced q_m by 50% for Kangilerngata and 10% for Umiamako.

In response to this forcing, Store, Rinks, and Kangerdlugssup have remained stable in ice front position, ice speed, and calving speed. We attribute the lack of retreat to the fact that q_m remains about 2–3 times lower than q_f for these glaciers, i.e., calving is the dominant ablation process. For an ice front to retreat ($q_r < 0$), the summer melt rate must at least exceed q_f, which was not the case during the entire period. In contrast, for the other two glaciers, the model simulation clearly suggests that summer melt rates regularly exceeded the ice speeds. For Kangilerngata, the melt speed exceeded the ice front speed around 2003 and the glacier retreat started in 2005. The glacier retreated in deeper waters, which increased the melt rate. The ice speed nearly tripled during that time and is now twice as large as the ocean-induced melt rate. For Umiamako, the summer melt rate exceeded the ice speed for several years, but the melt rate is only 1.5 m/d, so that the glacier could only retreat by a cumulative 50–100 m each summer. Its fast retreat started in 2002 as the winter melt matched the ice speed, i.e., enhanced ice melt retreated the ice front year round. The retreat peaked in 2005, at which point the glacier speed doubled, and the glacier has maintained a steady flow and ice front position in waters 50 m deeper.

These simulations indicate that glaciers dominated by calving processes are less sensitive to an increase in ocean temperature or subglacial runoff. For the other two glaciers, ice-ocean interaction dominates and the

glaciers had to retreat, as observed. Hence, the simulations explain why some glaciers retreated while others did not. For the glaciers that retreated, it provides a reasonable estimate of the timing of the retreat, i.e., when the annual melt rates increased above the ice speed. To extend the comparison further, we would need to model the time-dependent ice flow and calving dynamics of the glacier as in *Morlighem et al.* [2016].

If our calculations are correct, we can estimate how much the melt rates need to increase for Rinks, Store, and Kangerdlugssup to retreat. On Store, an increase of 50% would be necessary for q_m to approach q_f, whereas on Rinks and Kangerdlugssup q_m it would need to double. A doubling of q_m would require a substantial increase in subglacial water discharge and ocean temperature. We conclude that Rinks and Kangerdlugssup are the most stable glaciers among those studied here.

Our methodology is affected by a number of limitations beyond the uncertainty in TF, q_{sg}, and q_m. First is the issue of undercutting. The enhanced bending stress caused by undercutting decreases with time as ice viscously adjusts to bending [*Cook et al.*,2014; *Krug et al.*, 2014], so the impact of undercutting on iceberg calving will depend on the time separation between calving events and in particular should be less for glaciers that do not calve frequently. Second, the ice face is not vertical, e.g., Rinks develops a small floating section. A more horizontal ice face will yield lower melt rates under similar forcings. Third, we have few measurements to evaluate the model, especially in winter where the predicted rates are low yet significant. Fourth, surface thinning may also contribute to glacier retreat but is neglected here because the melt speed from the surface is 1 order of magnitude lower than that at the ice-ocean boundary.

Our approach for representing ice-ocean interaction at ice margins using equation (2) is applicable to other glaciers using reconstructions of ice sheet runoff and ocean temperature from RACMO2, ECCO2, or other models. This makes it possible to quantify the impact of these interactions over a broader range of glaciers and test other atmospheric and ocean models in Greenland. To do this, it will be necessary to collect bathymetry and ocean temperature data in other fjords. In situ observations of melt rates in both summer and winter are critically needed to evaluate and improve these models.

5. Conclusions

We present a detailed modeling of subaqueous melt rates of five major Greenland glaciers using reconstructions of subglacial freshwater flux, ocean thermal forcing, bathymetry, and bed geometry for the past two decades. The results reveal a significant seasonal variability in subaqueous melt rate in response to the seasonal variation in subglacial runoff and a significant increase in subaqueous melting in response to the increase in ice sheet runoff and ocean temperature. For three glaciers, this increase has not changed the balance between the calving rate and the rate of ocean-induced melt, so the glaciers have remained stable despite an increase in ice melt. For two others, the calculation unequivocally indicates that the melting speed was sufficient to dislodge the glaciers from their stable positions and trigger a glacier retreat which affected their flow speed and state of mass balance, especially when the glacier fronts retreated to deeper beds. We suggest that the recent and future evolution of other Greenland glaciers may be simulated in the same fashion, using simplified reconstructions of ocean-induced melt rates, and extended in the future with improved modelizations of ice-ocean interaction.

Acknowledgments
This work was performed at the University of California, Irvine, and at Caltechs Jet Propulsion Laboratory under a contract with the National Aeronautics and Space Administration Cryosphere Science Program (NNX13AI84A, NNX14AN03G, NNX14AB93G, and NNX12AB86G); the Modeling, Analysis, and Prediction Program; and the Gordon and Betty Moore Foundation (grant 3280). M.v.d.B. acknowledges funding from the Polar Program of the Netherlands Organization for Scientific Research (NWO) and the Netherlands Earth System Science Centre (NESSC). We thank Captain Milos Simovic of "Cape Race" and his crew for the 2013-2104 cruises and Captain Thorvald Jensen of the "Esle" and his crew for the 2012 cruise. A 100 m geotiff file of the bathymetry is available at ess.uci.edu/group/erignot/node/1535. ECCO2 data are posted on ecco2.jpl.nasa.gov. RACMO2 data are available upon request to M.v.d.B. Ice front shape files, drainage basins, and ice velocity data are available upon request to E.R.

References

Aschwanden, A., E. Bueler, C. Khroulev, and H. Blatter (2012), An enthalpy formulation for glaciers and ice sheets, *J. Glaciol.*, *58*, 441–457.
Benn, D. I., C. R. Warren, and R. H. Mottram (2007), Calving processes and the dynamics of calving glaciers, *Earth Sci. Rev.*, *82*(3), 143–179.
Bevan, S. L., A. Luckman, and T. Murray (2012), Glacier dynamics over the last quarter of a century at Helheim, Kangerdlugssuaq and 14 other major Greenland outlet glaciers, *Cryosphere*, *6*, 923–937.
Box, J. E., and D. T. Decker (2011), Greenland marine-terminating glacier area changes: 2000–2010, *Ann. Glaciol.*, *52*(59), 91–98.
Carbonnell, M., and A. Bauer (1968), Exploitation des couvertures photographiques aeriennes repetees du front des glaciers velant dans Disko Bugt et Umanak Fjord, Juin-Juillet 1964, *Medd. Groenl.*, *173*(5), 78.
Chauche, N., A. Hubbard, J.-C. Gascard, J. E. Box, R. Bates, M. Koppes, A. Sole, P. Christoffersen, and H. Patton (2014), Ice-ocean interaction and calving front morphology at two west Greenland tidewater outlet glaciers, *Cryosphere*, *8*, 1457–1468.
Christoffersen, P., R. I. Mugford, K. J. Heywood, I. Joughin, J. A. Dowdeswell, J. P. M. Syvitski, A. Luckman, and T. J. Benham (2011), Warming of waters in an East Greenland fjord prior to glacier retreat: Mechanisms and connection to large-scale atmospheric conditions, *Cryosphere*, *5*(3), 701–714.
Cook, S., I. C. Rutt, T. Murray, A. Luckman, T. Zwinger, N. Selmes, A. Goldscak, and T. D. James (2014), Modelling environmental influences on calving at Helheim Glacier in eastern Greenland, *Cryosphere*, *8*, 827–841.
Enderlin, E., and I. Howat (2013), Submarine melt rate estimates for floating termini of Greenland outlet glaciers (2000–2010), *J. Glaciol.*, *59*(213), 67–75.

Enderlin, E., I. M. Howat, S. Jeong, M. J. Noh, J. H. van Angelen, and M. R. van den Broeke (2014), An improved mass budget for the Greenland ice sheet, *Geophys. Res. Lett.*, *41*, 866–872, doi:10.1002/2013GL059010.

Ettema, J., M. R. van den Broeke, E. vanMeijgaard, W. J. van de Berg, J. L. Bamber, J. E. Box, and R. C. Bales (2009), Higher surface mass balance of the Greenland ice sheet revealed by high-resolution climate modelling, *Geophys. Res. Lett.*, *36*(12), L12501, doi:10.1029/2009GL038110.

Fried, M., G. Catania, T. Bartholomaus, D. Duncan, M. Davis, L. Stearns, J. Nash, E. Shroyer, and D. Sutherland (2015), Distributed subglacial discharge drives significant submarine melt at a Greenland tidewater glacier, *Geophys. Res. Lett.*, *42*, 9328–9336, doi:10.1002/2015GL065806.

Holland, D. M., R. H. Thomas, B. de Young, M. H. Ribergaard, and B. Lyberth (2008), Acceleration of Jakobshavn Isbr triggered by warm subsurface ocean waters, *Nat. Geosci.*, *1*(10), 659–664.

Howat, I. (2016), *MEaSURES Greenland Ice Velocity: Selected Glacier Site Velocity Maps From Optical Images, version 1*, NASA National Snow and Ice Data Center Distributed Active Archive Center, Boulder, Colo., doi:10.5067/EYV1IP7MUNSV.

Howat, I. M., J. E. Box, Y. Ahn, A. Herrington, and E. M. McFadden (2010), Seasonal variability in the dynamics of marine-terminating outlet glaciers in Greenland, *J. Glaciol.*, *56*(198), 601–613.

Joughin, I., B. Smith, I. Howat, T. Scambos, and T. Moon (2010), Greenland flow variability from ice sheet wide velocity mapping, *J. Glaciol.*, *56*(197), 415–430.

Kleiner, T., M. Ruckamp, J. H. Bondzio, and A. Humbert (2015), Enthalpy benchmark experiments for numerical ice sheet models, *Cryosphere*, *9*, 217–228.

Krug, J., J. Weiss, O. Gagliardino, and G. Durand (2014), Combining damage and fracture mechanics to model calving, *Cryosphere*, *8*, 2101–2117.

Losch, M., D. Menemenlis, P. Heimbach, J. Campin, and C. Hill (2010), On the formulation of sea-ice models. Part 1: Effects of different solver implementations and parameterizations, *Ocean Model*, *33*, 129–144.

Luckman, A., D. Benn, F. Cottier, S. Bevan, F. Nilsen, and M. Inall (2015), Calving rates at tidewater glaciers vary strongly with ocean temperature, *Nat. Comm.*, *6*, 8566, doi:10.1038/ncomms9566.

Moon, T., I. Joughin, B. Smith, and I. Howat (2012), 21st-century evolution of greenland outlet glacier velocities, *Science*, *336*, 576–578.

Morlighem, M., E. Rignot, J. Mouginot, H. Seroussi, and E. Larour (2014), Deeply incised submarine glacial valleys beneath the Greenland Ice Sheet, *Nat. Geosci.*, *7*, 418–422.

Morlighem, M., J. Bondzio, H. Seroussi, E. Rignot, E. Larour, A. Humbert, and S. Rebuffi (2016), Modeling of Store Gletscher's calving dynamics, West Greenland, in response to ocean thermal forcing, *Geophys. Res. Lett.*, *43*, 2659–2666, doi:10.1002/2016GL067695.

Motyka, R. J., M. Truffer, M. Fahnestock, J. Mortensen, S. Rysgaard, and I. Howat (2011), Submarine melting of the 1985 Jakobshavn Isbræ floating tongue and the triggering of the current retreat, *J. Geophys. Res.*, *116*, F01007, doi:10.1029/2009JF001632.

Nguyen, A., D. Menemenlis, and R. Kwok (2011), Arctic ice-ocean simulation with optimized model parameters: Approach and assessment, *J. Geophys. Res.*, *116*, C04025, doi:10.1029/2010JC006573.

Nguyen, A., R. Kwok, and D. Menemenlis (2012), Source and pathway of the Western Arctic upper halocline in a data-constrained coupled ocean and sea ice model, *J. Phys. Oceanogr.*, *43*, 802–823.

O'Leary, M., and P. Christoffersen (2013), Calving on tidewater glaciers amplified by submarine frontal melting, *Cryosphere*, *7*(1), 119–128.

Post, A., S. O'Neel, R. J. Motyka, and G. Streveler (2011), A complex relationship between calving glaciers and climate, *Eos Trans. AGU*, *92*(37), 305–306.

Rignot, E., and P. Kanagaratnam (2006), Changes in the velocity structure of the Greenland ice sheet, *Science*, *311*(5763), 986–990.

Rignot, E., and J. Mouginot (2012), Ice flow in Greenland for the International Polar Year 2008–2009, *Geophys. Res. Lett.*, *39*, L11501, doi:10.1029/2012GL051634.

Rignot, E., M. Koppes, and I. Velicogna (2010), Rapid submarine melting of the calving faces of west Greenland tidewater glaciers, *Nat. Geosci.*, *3*(3), 187–191.

Rignot, E., I. Fenty, D. Menemenlis, and Y. Xu (2012), Spreading of warm ocean waters around Greenland as a possible cause for glacier acceleration, *Ann. Glaciol.*, *53*(60), 257–266.

Rignot, E., I. Fenty, C. Kemp, X. Yun, and C. Cai (2015), Undercutting of Greenland marine-terminating glaciers in deep glacial fjords, *Geophys. Res. Lett.*, *42*, 5909–5917, doi:10.1002/2015GL064236.

Rignot, E., I. Fenty, Y. Xu, C. Cai, I. Velicogna, C. Ó. Cofaigh, J. A. Dowdeswell, W. Weinrebe, G. Catania, and D. Duncan (2016), Bathymetry data revealing glaciers vulnerable to ice-ocean interaction in Uummannaq and Vaigat glacial fjords, West Greenland, *Geophys. Res. Lett.*, *43*, 2667–2674, doi:10.1002/2016GL067832.

Seroussi, H., M. Morlighem, E. Rignot, A. Khazendar, E. Larour, and J. Mouginot (2013), Dependence of century-scale projections of the Greenland ice sheet on its thermal regime, *J. Glaciol.*, *59*, 1024–1034.

Slater, D. A., P. W. Nienow, T. R. Cowton, D. N. Goldberg, and A. J. Sole (2015), Effect of near-terminus subglacial hydrology on tidewater glacier submarine melt rates, *Geophys. Res. Lett.*, *42*, 2861–2868, doi:10.1002/2014GL062494.

Straneo, F., S. H. Gordon, D. A. Sutherland, L. A. Stearns, F. Davidson, M. O. Hammill, G. B. Stenson, and A. Rosing-Asvid (2010), Rapid circulation of warm subtropical waters in a major, East Greenland glacial fjord, *Nat. Geosci.*, *3*, 182–186.

Sutherland, D., and F. Straneo (2012), Estimating ocean heat transports and submarine melt rates in Sermilik Fjord, Greenland, using lowered acoustic Doppler current profiler (LADCP) velocity profiles, *Ann. Glaciol.*, *53*(60), 50–58.

van Angelen, J., et al. (2012), Sensitivity of Greenland ice sheet surface mass balance to surface albedo parameterization: A study with a regional climate model, *Cryosphere*, *6*, 1175–1186.

van den Broeke, M., et al. (2009), Partitioning recent Greenland mass loss, *Science*, *326*(5955), 984–986.

Weidick, A. (1968), Observations on some Holocene glacier fluctuations in West Greenland, *Meddelelser om Grønland*, *165*, 1–202.

Weinrebe, R. W., A. Kuijpers, I. Klaucke, and M. Fink (2009), Multibeam bathymetry surveys in Fjords and coastal areas of West-Greenland, *Eos Trans. AGU*, *90*(52), Fall Meet. Suppl., Abstract OS21A–1152.

Xu, Y., E. Rignot, I. Fenty, D. Menemenlis, and M. Mar Flexas (2013), Subaqueous melting of Store Glacier, West Greenland from three-dimensional, high-resolution numerical modeling and ocean observations, *Geophys. Res. Lett.*, *40*, 4648–4653, doi:10.1002/grl.50825.